Journal of Saudi Chemical Society (2020) **24**, 857–864

King Saud University

Journal of Saudi Chemical Society

www.ksu.edu.sa
www.sciencedirect.com

ORIGINAL ARTICLE

Co-doping with boron and nitrogen impurities in T-carbon

Zhen-Wei Tian [a,1], Xiao-Qian Cui [a,1], Jia-Kun Tian [a], Mu-Chen Cui [a], Li Jin [b], Ran Jia [c,d,*], Roberts I. Eglitis [d]

[a] *Department of Emergency and Critical Care, The Second Hospital of Jilin University, 130023 Changchun, PR China*
[b] *Anshan Tumor Hospital, 114034 Anshan, PR China*
[c] *Institute of Theoretical Chemistry, Jilin University, 130023 Changchun, PR China*
[d] *Institute of Solid State Physics, University of Latvia, 8 Kengaraga Str., Riga LV1067, Latvia*

Received 10 August 2020; revised 25 August 2020; accepted 6 September 2020
Available online 20 September 2020

KEYWORDS

T-carbon;
Doping;
BN pair;
DFT

Abstract Previously, Ren et al. [Chem. Phys. 518, 69–73, 2019] reported the failure of Boron-Nitrogen (B-N) co-doping as inter B-N bond in T-carbon. In present work, a B-N atom pair is introduced in T-carbon as p-n co-dopant to substitute two carbon atoms in the same carbon tetrahedron and form an intra B-N bond. The stability of this doping system is verified from energy, lattice dynamic, and thermodynamic aspects. According to our B3PW calculations, B-N impurities in this situation can reduce the band gap of T-carbon from 2.95 eV to 2.55 eV, making this material to be a promising photocatalyst. Through the study of its transport properties, we can also conclude that B-N co-doping cannot improve the thermoelectric performance of T-carbon.

1. Introduction

A novel carbon allotrope, T-carbon, had been firstly predicted by computer simulation [1], before it was successfully synthesized [2,3]. After that, many theoretical studies for the mechanic and electronic features of the pristine T-carbon system had been reported [4–10]. Similar to cubic diamond, another metastable carbon allotrope, the carbon atoms in T-carbon are all sp^3 hybridized forming carbon tetrahedrons which are arranged still following the Fd-3 m symmetry. In order to promote the further research of T-carbon, Su et al. proposed two promising applications for superconducting via sodium doping [11] and novel energy systems (e.g., thermoelectrics, hydrogen storage, and lithium ion batteries) [12].

Usually, doping is the most common and effective method for artificially manipulating the electronic structures of the research materials [13–17]. For instance, point defects with heteroatom in diamond are very common, which leads to the attractive colors of diamond. More importantly, the state of the negatively charged nitrogen-vacancy defect in diamond

* Corresponding author at: Institute of Theoretical Chemistry, Jilin University, 130023 Changchun, PR China.
E-mail address: jiaran@jlu.edu.cn (R. Jia).
[1] These authors contributed equally to this work and should be considered as co-first authors.
Peer review under responsibility of King Saud University.

Production and hosting by Elsevier

https://doi.org/10.1016/j.jscs.2020.09.002

[18] can now be read out by photoelectric detection methods [19]. Therefore, this optically active center could be a promising candidate as spin qubit in quantum computation [20]. However, it is not a very easy task to introduce heteroatoms into T-carbon due to its bond angles which are far from the perfect sp^3 hybridization, and the consequent internal stress. Ren and co-workers assessed different categories of doped T-carbon by using DFT calculations [21]. Their simulation results show that the single B or N dopant in T-carbon will lead to the presence of the soft modes in their phonon distribution maps. They also claimed that the substitution of two carbon atoms in two neighboring tetrahedrons by a B-N co-dopant would cause the instability of the face-centered cubic system, too. Unfortunately, we didn't find the evidence in their work for the last conclusion, which aroused our interest. Therefore, two different configurations for B-N co-doping in T-carbon are considered in this study: i. B and N atoms are introduced in two neighboring tetrahedrons replacing two C atoms to form an inter-tetrahedron B-N bond; ii. B and N atoms substitute two C atoms in a same tetrahedron to form an intra-tetrahedron B-N bond. Here, we label them as T-CBN1 and T-CBN2 for inter and intra doping, respectively. According to our calculations, the shapes of the unit cells of both two doped systems are changed after full relaxations. The inter B-N doping system T-CBN1 is indeed unstable, which confirms the literature report [21]. However, the intra B-N doping system T-CBN2 could be stable. The intra B-N co-doping will not significantly weaken the mechanical moduli, while it can reduced the electronic energy band gap to around 2.55 eV. Hence, it might be possible to bring this material system into new application fields.

In present work, the stability of the T-CBN2 system will be verified from the energetic, lattice dynamic, and thermodynamic perspectives. The atomic and electronic configurations will also be presented. The change of the transport properties (i.e., electron conductivity, Seebeck coefficient, and electronic thermal conductivity) due to the B-N co-doping will be discussed. A short statement will be given as brief summary at the end of this work.

2. Computational details

The simulations in this study were performed with the help of the density functional theory (DFT) at the Perdew-Burke-Ernzerhof (PBE) [23] and global hybrid functional B3PW [24] levels as implemented in the computer code CRYSTAL17 [25,26]. Note that in order to obtain a reasonable band gap of the T-carbon and its doping systems, only 10% mixing of exact Hartree-Fock exchange was used in B3PW functional. This mixing parameter was verified by comparing the calculated band gap of T-carbon with the values reported in the original work (2.97 eV) by Su [1] and from our G_0W_0 calculation (2.94 eV). Other common functionals, e.g., B3LYP, PBE0, HSE06, and B1WC, were also tested. The differences among the results from these functionals can be found in Table 1. The all-electron Gaussian basis set Triple-Zeta Valence with Polarization (TZVP) [27] was employed for all species in the systems. After careful testing, a very dense 64 × 64 × 64 Monkhorst-Pack (MP) k-points grid was employed for the integration in the first Brillouin zone in order to ensure the accuracy of the calculated geometric and electronic configurations.

The thermal stability of the intra B-N doping system was affirmed by ab-initio molecular dynamics (AIMD) simulations with the aid of the computer code CASTEP [28]. The canonical ensembles at different temperatures were employed for 200 ps AIMD simulation with a time step 0.1 fs. Here, the norm-conserving pseodopotentials were chosen for the species in the simulation box.

The transport properties, e.g., electron conductivity σ, Seebeck constant S, and electronic thermal conductivity κ_{el}, were also investigated by solving the semiclassical Boltzmann transport equation. Firstly, the transport distribution function was estimated by using the following equation:

$$\Xi_{qr}(\epsilon) = \tau \sum_{\vec{k}} \frac{1}{N_{\vec{k}}} \frac{1}{V} \sum_{i,j} v_{i,q}(\vec{k}) v_{j,r}(\vec{k}) \delta(\epsilon - \epsilon_i(k)) \quad (1)$$

Table 1 The densities ρ in units of g/cm^3, cohesive energies E_{coh} and formation energies E_{form} in eV/atom, and band gaps E_g in eV of the pristine T-carbon and the intra BN doped T-carbon (T-CBN2), and their bulk modulus B, shear modulus G, Young's modulus Y, Poisson's ratio ν. Note that the mechanical moduli are all in units of GPa.

		ρ	E_{coh}	E_{form}	E_g	B	G	Y	ν
T-CARBON	PBE [22]	1.53	−7.63	–	2.20	165.67	45.99	126.27	0.373
	B3PW	1.53	−8.14	–	2.95	167.47	49.47	135.79	0.365
	B3LYP	1.54	−8.04	–	3.72	170.11	47.74	130.97	0.372
	B1WC	1.55	−9.40	–	3.35	174.35	50.45	138.05	0.368
	HSE06	1.55	−8.96	–	3.44	175.70	51.47	140.68	0.367
	PBE0	1.55	−9.50	–	4.04	175.32	51.35	140.36	0.367
	GGA [1]	1.50	−6.57	–	2.25	169	70	–	–
	PBE [21]	–	−7.84	–	2.25	161	48	–	–
	EXP. [2]	–	–	–	5.10	–	–	–	–
T-CBN2	PBE	1.53	−7.47	0.29	1.77	132.33	40.40	102.02	0.361
	B3PW	1.53	−7.96	0.13	2.55	137.77	43.33	117.38	0.358
	B3LYP	1.53	−7.90	0.18	3.40	137.92	42.83	116.43	0.359
	B1WC	1.55	−9.11	0.13	3.04	143.17	44.42	120.78	0.359
	HSE06	1.56	−8.83	0.16	3.18	143.84	45.09	122.47	0.358
	PBE0	1.56	−9.36	0.14	3.81	143.85	45.01	122.28	0.358

with the electron velocity $v_{i,q}(\vec{k})$ of the i-th band along the direction q and the lifetime τ. In the relaxation time approximation, a constant lifetime τ was chosen to be 10 fs in this work. Then, σ, σS and κ_{el} can be obtained from Boltzmann's semiclassical transport theory with the estimated $\Xi_{qr}(\epsilon)$:

$$[\sigma]_{qr} = \int dE\left(-\frac{\partial f_0}{\partial E}\right)\Xi_{qr}(\epsilon), \tag{2}$$

$$[\sigma S]_{qr} = \frac{1}{T}\int dE\left(-\frac{\partial f_0}{\partial E}\right)(E-\mu)\Xi_{qr}(\epsilon), \tag{3}$$

$$[\kappa_{el}]_{qr} = \frac{1}{T}\int dE\left(-\frac{\partial f_0}{\partial E}\right)(E-\mu)^2\Xi_{qr}(\epsilon), \tag{4}$$

where μ is the chemical potential, and f_0 is the Fermi-Dirac distribution [29].

3. Results and discussion

3.1. Geometric configurations

The pristine T-carbon, as shown in Fig. 1(a), possesses the similar structure of cubic diamond (c-diamond), but based on carbon tetrahedron instead of single carbon atom. Our calculated lattice constants of T-carbon are 7.473 Å and 7.469 Å at PBE and B3PW levels, respectively, which are all in good agreement with the literature value 7.52 Å [1]. There are two different C–C bonds in T-carbon. Therefore, we consider two different B-N arrangements in this work. Their doping positions are exhibited in Fig. 1(b). Here, the system with inter B-N bond between two neighboring tetrahedrons is named as T-CBN1, and in the other case, the system with intra B-N bond in the same tetrahedron is called T-CBN2. Note that we just attempt to demonstrate the doping positions in Fig. 1(b). Their doping concentration are 25%. After full relaxations, the geometric configurations, even the space

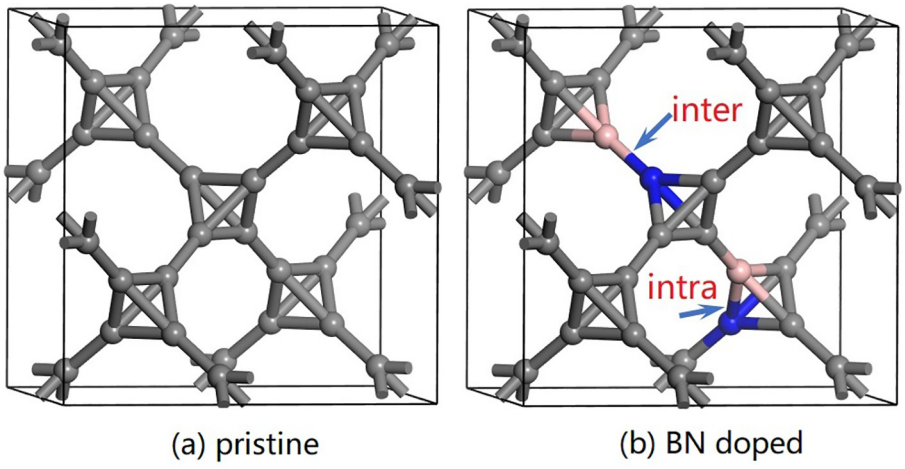

Fig. 1 (a) Atomic configurations for pristine T-carbon, and (b) the sketch of the B-N doping positions in T-carbon. Note that the geometric configurations will be totally changed after B-N co-doping, including the space group, the lattice parameters, and the bonds. Here, we illustrate the atomic sketch of the doping system before the geometry relaxations in order to clearly show the different doping arrangements. Note that the gray, blue, and pink spheres are represented for carbon, nitrogen, and boron atoms, respectively.

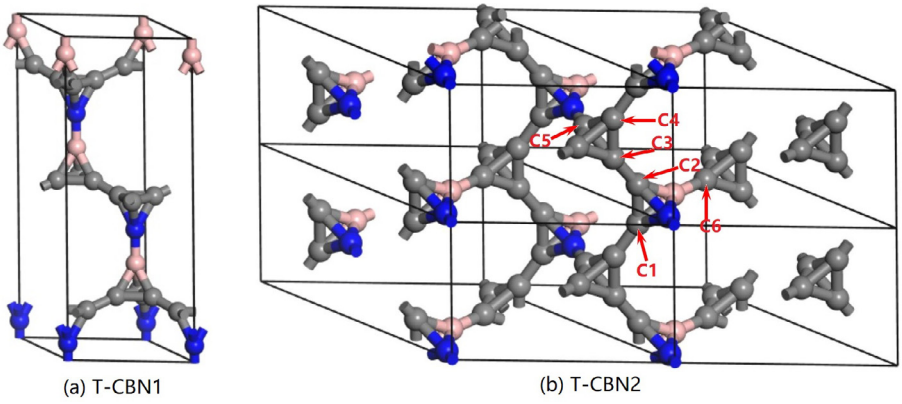

Fig. 2 Atomic configurations for (a) inter and (b) intra B-N co-doped T-carbon (T-CBN1 and T-CBN2, respectively) after full relaxations. As define in Fig. 1, the gray, blue, and pink spheres are represented for carbon, nitrogen, and boron atoms, respectively.

groups, of these doping systems are obviously changed as shown in Fig. 2. In the first case, T-CBN1 becomes to be trigonal along R3m symmetry with the lattice constants a = b = 5.24 Å and c = 13.54 Å at PBE level. The fully relaxed T-CBN2 by using PBE functional possesses even less symmetry operators with monoclinic lattice Cm where a = 5.23 Å, b = 7.47 Å, c = 8.57 Å, α = β = 90°, and γ = 140.90°.

The first concern is the stability of the doped T-carbon systems, which is also the initial motivation of this study. The phonon dispersion maps in Fig. 3 show clear soft modes in T-CBN1 system, but not in T-CBN2. Therefore, the B-N doping in two neighboring tetrahedrons to form a inter B-N bond will cause the instability of the T-carbon system. The phonon dispersion relation provides an evidence of the lattice dynamic stability of the intra tetrahedron B-N co-doping system T-CBN2, which was not considered in the literature [21]. Future AIMD simulations confirm the thermal stability of T-CBN2. As plotted in Fig. 4, the crystal structure of T-CBN2 has no significant distortion at least up to 600 K in 20 ps. In terms of energy, the cohesive energy can be estimated as the summation of the chemical potentials of all atoms:

$$E_{coh} = \frac{1}{n}\sum_i n_i\mu_i, \tag{5}$$

where μ_i represents the chemical potential of particular species i, n_i is the number of the i-th specie. n is the total number of the atoms in the system. The cohesive energies of the pristine T-carbon and T-CBN2 are listed in Table 1. B-N co-doping in the same tetrahedron of T-carbon leads to only around 200 meV energy rise. Usually, it will take a certain amount of energy to form a defect or introducing impurities in crystal. The formation energy of T-CBN2 system can be defined as follows:

$$E_{form} = \frac{1}{8}(E_{new} + 2\mu_C - E_{old} - \mu_B - \mu_N). \tag{6}$$

According this definition, the formation energy of T-CBN2 is up to 0.3 eV depending on the functional employed in the calculation, as listed in Table 1. At PBE and B3PW levels, the formation energies E_{form} are around 0.16 eV (3.79 kcal/mol) and 0.18 eV (4.16 kcal/mol), respectively. So, the formation of the B-N doping in a same tetrahedron of T-carbon should not be very energy consuming. Therefore, we would like to suggest that T-CBN2 system could be stable from lattice dynamic, thermodynamic, and energetic aspects.

From here on out, only the intra doping case T-CBN2 will be discussed. There are two different C–C bonds (i.e., inter and intra bonds) in pristine T-carbon with the bond lengths 1.408 Å and 1.492 Å, respectively, according to our PBE calculation. The introduction of B-N impurities in a tetrahedron of the unit cell of T-carbon leads to significant deformation and symmetry reduction. In Fig. 2(b), the carbon atoms are labeled with numbers in order to conveniently name the different chemical bonds. There are three different inter bonds between

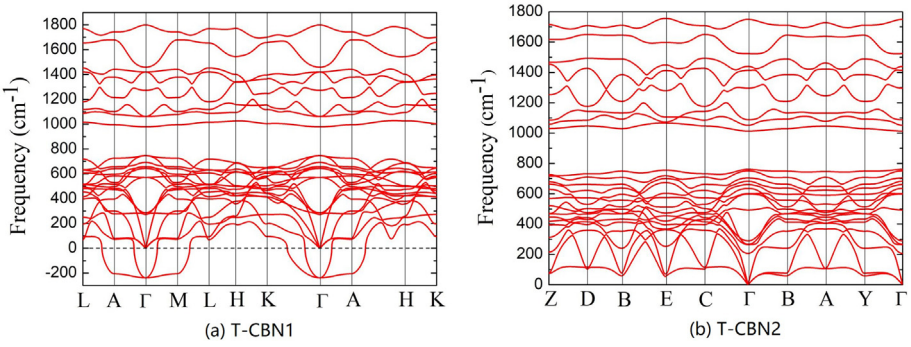

Fig. 3 The phonon dispersion maps for (a) T-CBN1, and (b) T-CBN2.

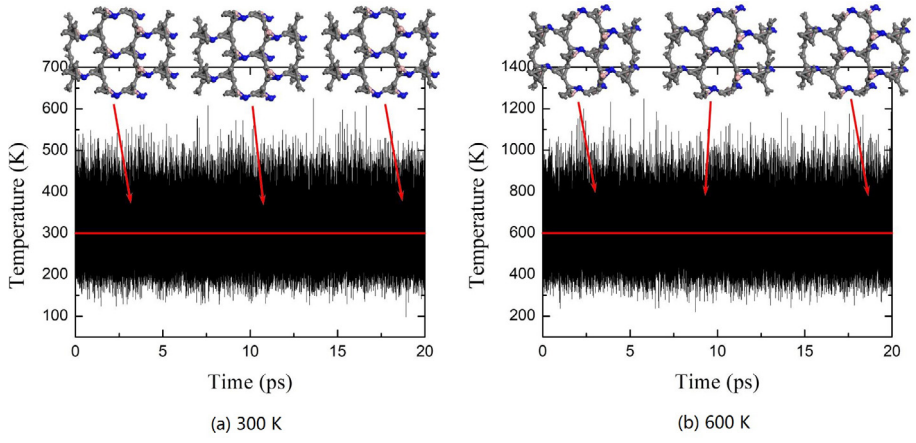

Fig. 4 AIMD simulation results in canonic ensembles at (a) 300 K, and (b) 600 K.

two neighboring tetrahedrons, namely B-C6, N-C5, and C2-C3 which are 1.501 Å, 1.363 Å, and 1.405 Å, respectively. Note that C1 and C2 in the doped tetrahedron are equivalent. There are four nonequivalent bonds in doped tetrahedron: B-C1(↔B-C2) = 1.548 Å, N-C1(↔N-C2) = 1.546 Å, C1-C2 = 1.486 Å, and B-N = 1.572 Å. The N-C1 bond is only a little shorter than B-C1. In the undoped carbon tetrahedron, there are six C–C bands with four different bond lengths: C3-C4 =

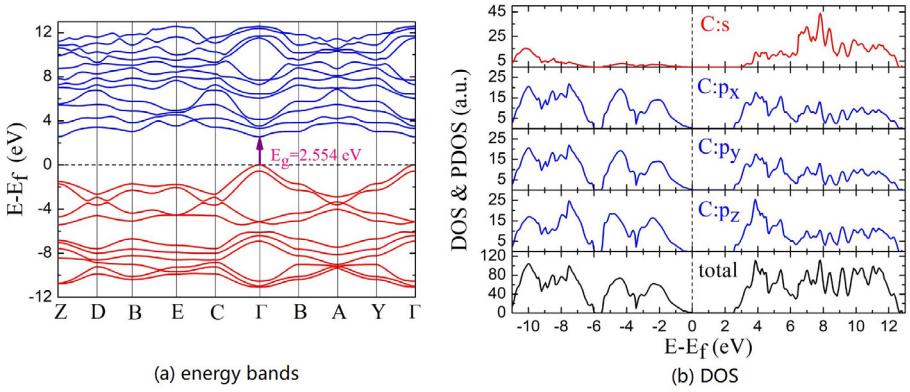

Fig. 5 (a) The calculated electronic energy band structure of T-CBN2 at B3PW level, and (b) the DOS map and its projection onto C-atoms. Note that the Fermi level is shifted to zero and indicated by dotted lines. The other PDOS maps can be found in Figs. S1–S4.

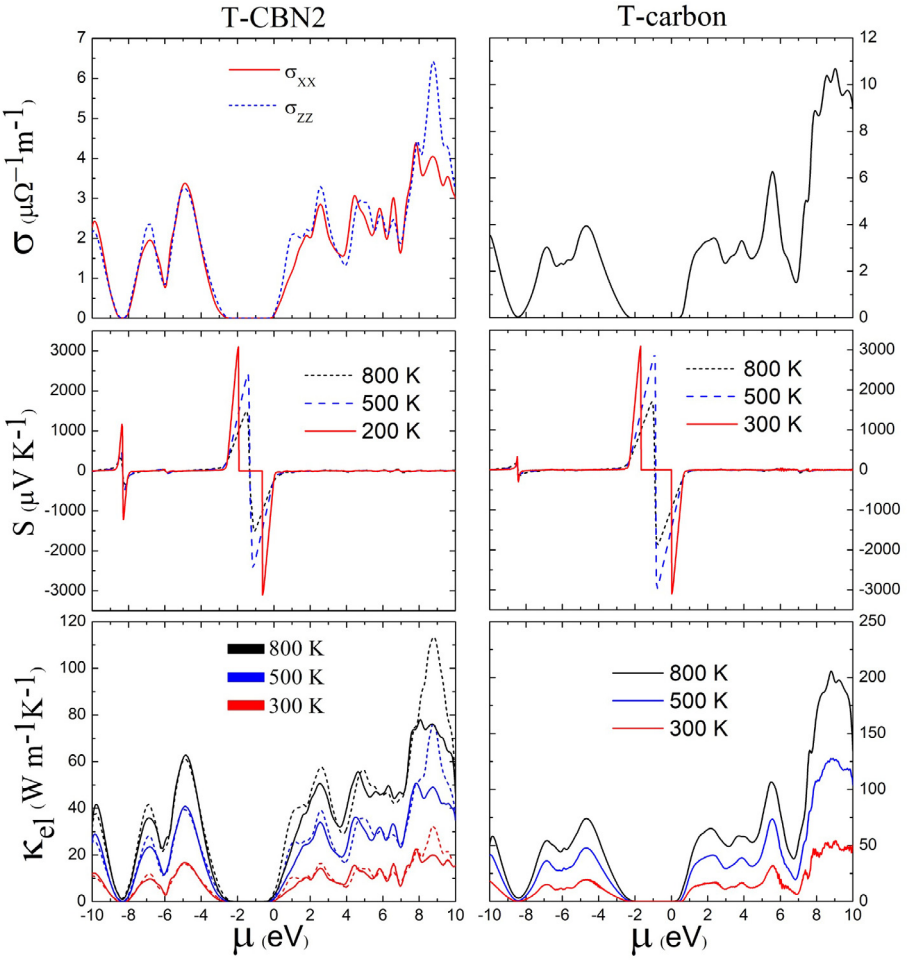

Fig. 6 The calculated electron conductivities σ, Seebeck coefficients *S*, and electronic thermal conductivities κ_{el} of T-CBN2 and pristine T-carbon as functions of chemical potential μ at B3PW level. The calculated Fermi-level of T-CBN2 is located at −2.563 eV. The solid and dashed lines exhibit the electronic thermal conductivity elements κ_{xx} and κ_{zz} of T-CBN2 in the lower left panel, respectively. Note that these calculations are performed with τ = 10 fs in the constant relaxation time approximation as defined in Eq. (1).

1.485 Å, C5-C6 = 1.482 Å, C3-C5(↔C4-C5) = 1.475 Å, and C3-C6(↔C4-C6) = 1.526 Å. The bond length of inter C2-C3 is 1.405 Å which is very close to the original inter bond length in pristine T-carbon. Note that C3 and C4 in the undoped tetrahedron are also equivalent. As a consequence of the changes of the atomic and electronic configurations, the bulk modulus of T-CBN2 is about 20% lower than that of pristine T-carbon. Due to the slight decrease of the Poisson's ratio, the attenuations of the Young's and shear moduli of the B-N doping system are not as large as bulk modulus. The detailed information of the mechanical properties of T-carbon and T-CBN2 can be found in Table 1, too.

3.2. Electronic configuration

According to the literature [21], T-carbon is a semiconductor with 3.0 eV direct band gap determined at B3LYP level. From our calculations by using different DFT levels as listed in Table 1, one can see that the B3PW value is very close to previous theoretical prediction. Therefore, only B3PW results will be mentioned in the following discussion about the electronic configuration of T-CBN2 system. Note that there is only 10% mixing of exact Hartree-Fock exchange in this setting instead of the original B3PW setting with 20%.

After introducing a B-N pair into T-carbon unit cell, the electrons in the system will be redistribute. Mulliken's analysis shows that the N atom accepts 0.85 electrons from its neighboring atoms. Sequentially, the effective charges of the N dopant are − 3.85 e, now. The B and C5 atoms donate 0.67 and 0.46 electrons, respectively. On the contrary, the C6 atom which forms inter bond with the B atom obtains 0.25 electrons. The Mulliken's bond overlap populations on the inter and intra C–C bonds in pristine T-carbon are 0.46 and 0.18 electrons. In T-CBN2 system, the Mulliken's bond overlap population on the inter C2-C3 bond is obviously weakened to 0.40 electrons. The bond overlap populations on other intra C–C bonds are all slightly weakened leading to the reduction of the mechanical stiffness. Although the bond overlap population on B-N bond is still 0.17 electrons, there is also Coulomb interaction between B and N atoms showing some ionic bond features.

The band gap of T-CBN2 is reduced from around 3.0 eV of T-carbon to 2.55 eV at B3PW level. The direct band gap is still located at Γ point. The details of the band structure of T-CBN2 can be found in Fig. 5(a). The conduction band edge around Γ point are obviously flatter than the valence band edge, which indicates that the effective mass of an electron hole at valence band maximum (VBM) should be significantly smaller than that of an electron at conduction band minimum (CBM). According to the following equation:

$$\frac{1}{m^*} = \frac{1}{\hbar^2}\left(\frac{\partial^2 E}{\partial k^2}\right), \tag{7}$$

the effective masses of electron and electron hole at CBM and VBM are 0.14 m_e and 0.10 m_e, respectively. This difference may help the separation of the charge carriers in T-CBN2 system. From the density of states (DOS) maps illustrated in Fig. 5(b), one can find that the edges of the valence bands and conduction bands consist of the p orbitals of the carbon atoms. As reported in previous work [1], the carbon atoms in T-carbon are all sp^3 hybridized. However, in T-CBN2, the projected DOS curves of the carbon atoms are not all identical near the Fermi level, which points out the partial sp^2 hybridization characteristics of the carbon atoms after electron redistribution due to B-N doping. The DOS diagrams for

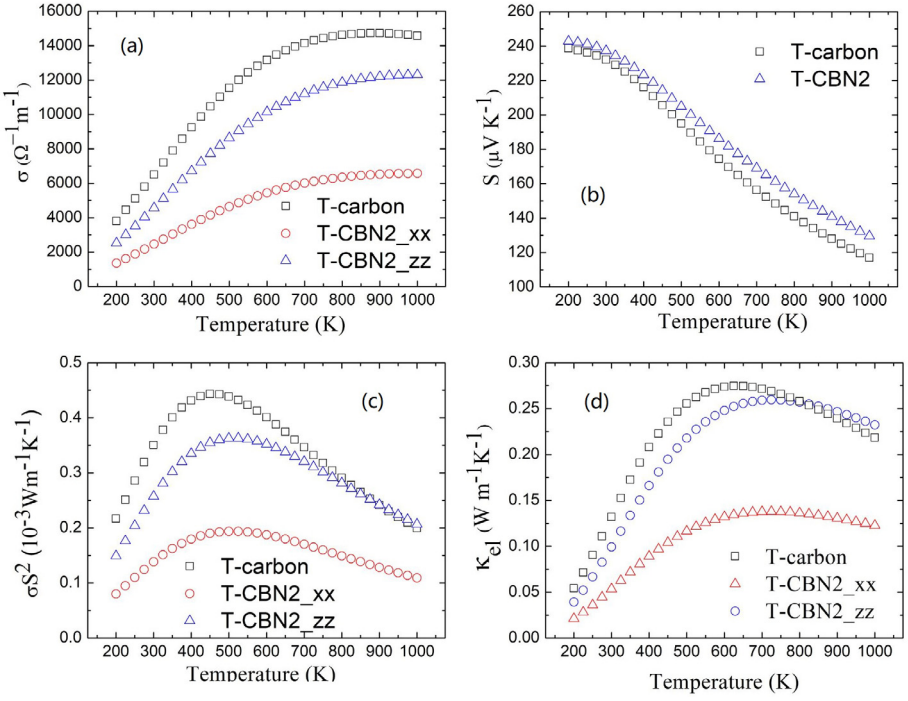

Fig. 7 The transport properties of T-CBN2 and pristine T-carbon at their Fermi levels as functions of temperature: (a) electronic conductivities, (b) Seebeck coefficients, (c) thermoelectric power factors, and (d) electronic thermal conductivities.

particular C, B, and N atoms are illustrated in Supporting Information.

3.3. Transport properties

Previously, Su et al. proposed the application potential of T-carbon as a thermoelectric material [11]. Thermoelectricity of a material is actually determined by its transport properties, i.e., electronic conductivity σ, Seebeck coefficient S, and thermal conductivity κ. Doping will significantly change σ and κ owing to the scattering effect around the impurity atoms. Once the transport distribution function as defined in Eq. (1) is determined, σ, S, and electronic thermal conductivity κ_{el}can be estimated via semiclassical Boltzmann's transport theory. The electronic conductivity σ of T-CBN2 is clearly lower than that of T-carbon. Moreover, σ of T-CBN2 emerges certain anisotropy as exhibited in Fig. 6(a). Different from the other two transport parameters, temperature has relatively mild effect on σ. The Seebeck coefficient S near the Fermi level has not been greatly influenced by the B-N impurities, as shown in Fig. 6(b). At very low chemical potential (around − 8.5 eV), S of T-CBN2 is obviously enhanced comparing with T-carbon. The peaks near the Fermi level on the curves of S become higher and narrower with the increasing temperature. Commonly, the thermal conductivity can be separated into two parts: $\kappa = \kappa_{el} + \kappa_l$, where the first term represents the electronic contribution, and the second one is the contribution of the lattice vibration. Similar to the electronic conductivity, the electronic thermal conductivity κ_{el} of T-CBN2 exhibits some anisotropy as shown in Fig. 6(c).

Fig. 7 clearly exhibits the relationships between the transport properties and temperature at the Fermi levels of T-carbon and T-CBN2. Except the Seebeck coefficient, the other two transport properties σ and κ_{el} are obviously anisotropic at Fermi level after B-N doping. The slight enhanced Seebeck coefficient of T-CBN2 cannot offset the reduction of the electronic conductivity at Fermi level. Therefore, the thermoelectric power factor of T-CBN2 is still smaller than that of pristine T-carbon at Fermi levels. As reported in previous work [6], the lattice thermal conductivity κ_l of T-carbon is around 33 W/mK at 300 K, which means that the thermal conductivity of T-carbon is dominated by κ_l. From this point, we can conclude that B-N doping in T-carbon cannot improve its thermoelectric property.

4. Conclusion

In summary, a doping structure with B-N impurities in T-carbon is found, namely T-CBN2. The B-N impurities, as p-n co-dopant, can substitute two carbon atoms in the same tetrahedron to form an intra B-N bond, instead of an inter B-N bond. Its lattice dynamic and thermal stabilities are verified by performing the calculations for its phonon dispersion relation and AIMD at different temperatures. The B-N co-doping strongly changes the atomic and electronic configurations of T-carbon. The mechanic properties are mildly reduced. The band gap is also reduced from 2.95 eV to 2.55 eV owing to the electron redistribution after B-N doping, according to our B3PW calculations. The transport properties: σ, S, and κ_{el} are also investigated. Our calculation results do not support improvement of the thermoelectric capability of T-carbon by B-N co-doping. Although the B-N doped T-carbon is unlikely to be used as thermoelectric material, its stable structure, good mechanical properties, and proper band gap indicate that this material is a promising photocatalyst. The polarized B-N bond and relatively larger geometric channels in T-CBN2 also indicate its potential applications in gas adsorption and separation fields.

Appendix A. Supplementary data

Supplementary data to this article can be found online at https://doi.org/10.1016/j.jscs.2020.09.002.

References

[1] X.-L. Sheng, Q.-B. Yan, F. Ye, Q.-R. Zheng, G. Su, T-carbon: A novel carbon allotrope, Phys. Rev. Lett. 106 (2011) 155703.

[2] J. Zhang, R. Wang, X. Zhu, A. Pan, C. Han, X. Li, D. Zhao, C. Ma, W. Wang, H. Su, C. Niu, Pseudo-topotactic conversion of carbon nanotubes to T-carbon nanowires under picosecond laser irradiation in methanol, Nat. Commun. 8 (2017) 683.

[3] K. Xu, H. Liu, Y. Shi, J. You, X. Ma, H. Cui, Q. Yan, G. Chen, G. Su, Preparation of T-carbon by plasma enhanced chemical vapor deposition, Carbon 157 (2020) 270–276.

[4] X. Chen, H. Niu, C. Franchini, D. Li, Y. Li, Hardness of T-carbon: Density functional theory calculations, Phys. Rev. B 84 (2011) 121405(R).

[5] J.Y. Jo, B.G. Kim, Carbon allotropes with triple bond predicted by first-principle calculation: Triple bond modified diamond and T-carbon, Phys. Rev. B 86 (2012) 075151.

[6] S. Yue, G. Qin, X. Zhang, X. Sheng, G. Su, M. Hu, Thermal transport in novel carbon allotropes with sp^2 or sp^3 hybridization: An ab initio study, Phys. Rev. B 95 (2017) 085207.

[7] L. Bai, P. Sun, B. Liu, Z. Liu, K. Zhou, Mechanical behaviors of T-carbon: A molecular dynamics study, Carbon 138 (2018) 357–362.

[8] X. Bu, S. Wang, Electron-phonon scattering and excitonic effects in T-carbon, RSC Adv. 10 (2020) 24515.

[9] Y. Wang, J. Lei, L. Bai, K. Zhou, Z. Liu, Effects of tensile strain rate and grain size on the mechanical properties of nanocrystalline T-carbon, Comput. Mater. Sci. 170 (2019) 109188.

[10] H. Alborznia, M. Naseri, N. Fatahi, Pressure effects on the optical and electronic aspects of T-carbon: A first principles calculation, Optik 180 (2019) 125–133.

[11] J. You, B. Gu, G. Su, Superconductivity in sodium-doped T-carbon, Phys. Rev. B 101 (2020) 184521.

[12] G. Qin, K. Hao, Q. Yan, M. Hu, G. Su, Exploring T-carbon for energy applications, Nanoscale 11 (2019) 5798.

[13] R. Jia, H. Shi, G. Borstel, First-principles calculations of oxygen-vacancy dipoles and hydrogen impurities in SrF_2, Phys. Rev. B 78 (2008) 224101.

[14] L. Miao, R. Jia, Y. Wang, C. Kong, J. Wang, R.I. Eglitis, H. Zhang, Certain doping concentrations caused half-metallic graphene, J. Saudi Chem. Soc. 21 (2017) 111–117.

[15] M. Green, Z. Liu, P. Xiang, Y. Liu, M. Zhou, X. Tan, F. Huang, L. Liu, X. Chen, Doped, conductive SiO_2 nanoparticles for large microwave absorption, Light: Sci. Appl. 7 (2018) 87.

[16] C. Stihler, C. Jauregui, A. Tünnermann, J. Limpert, Modal energy transfer by thermally induced refractive index gratings in Yb-doped fibers, Light: Sci. Appl. 7 (2018) 59.

[17] D. Yang, Z. Tian, Y. Chen, R.I. Eglitis, H. Zhang, R. Jia, Giant piezoelectricity in B/N doped 4,12,2-graphyne, Appl. Surf. Sci. 499 (2020) 143800.

[18] A. Gali, E. Janzén, P. Deák, G. Kresse, E. Kaxiras, Giant theory of spin-conserving excitation of the N-V^- center in diamond, Phys. Rev. Lett. 103 (2009).
[19] E. Bourgeois, M. Gulka, M. Nesladek, Photoelectric detection and quantum readout of nitrogen-vacancy center spin states in diamond, Adv. Opt. Mater. 8 (2020) 1902132.
[20] S. Prawer, A.D. Greentree, Diamond for quantum computing, Science 320 (2008) 1601–1602.
[21] H. Ren, H. Chu, Z. Li, T. Yue, Z. Hu, Efficient energy gap tuning for T-carbon via single atomic doping, Chem. Phys. 518 (2019) 69–73.
[22] J. Zhou, L. Li, C. Fu, J. Wang, P. Fu, C. Kong, F. Bai, R.I. Eglitis, H. Zhang, R. Jia, A novel T-C_3N and seawater desalination, Nanoscale 12 (2020) 5055.
[23] J.P. Perdew, K. Burke, M. Ernzerhof, Generalized gradient approximation made simple, Phys. Rev. Lett. 77 (1996) 3865–3868.
[24] A.D. Becke, Density-functional thermochemistry. III The role of exact exchange, J. Chem. Phys. 98 (1993) 5648.
[25] A. Erba, J. Baima, I. Bush, R. Orlando, R. Dovesi, Large-scale condensed matter DFT simulations: performance and capabilities of the CRYSTAL code, J. Chem. Theory Comput. 13 (2017) 5019–5027.
[26] R. Dovesi, V.R. Saunders, C. Roetti, R. Orlando, C.M. Zicovich-Wilson, F. Pascale, B. Civalleri, K. Doll, N.M. Harrison, I.J. Bush, Ph. D'Arco, M. Llunel, M. Causà, Y. Noël, L. Maschio, A. Erba, M. Rérat, S. Casassa, Large-Scale Condensed Matter DFT Simulations: Performance and Capabilities of the CRYSTAL Code, CRYSTAL17 User's Manual, University of Torino, Torino, 2017.
[27] M.F. Peintinger, D.V. Oliveira, T. Bredow, Consistent gaussian basis sets of triple-zeta valence with polarization quality for solid-state calculations, J. Comp. Chem. 34 (2013) 451–459.
[28] S.J. Clark, M.D. Segall, C.J. Pickard, P.J. Hasnip, M.J. Probert, K. Refson, M.C. Payne, First principles methods using CASTEP, Z. für Krist. 220 (2005) 567–570.
[29] G. Sansone, A. Ferretti, L. Maschio, Ab inito electronic transport and thermoelectric properties of solids from full and range-separated hybrid functionals, J. Chem. Phys. 147 (2017) 114101.